



Electro-chemo-mechanical coupling in structural lithium-ion batteries: Experimental findings and numerical modelling

Downloaded from: <https://research.chalmers.se>, 2025-12-17 09:44 UTC

Citation for the original published paper (version of record):

Al-Emrani, R., Larsson, C., Dahlberg, C. et al (2026). Electro-chemo-mechanical coupling in structural lithium-ion batteries: Experimental findings and numerical modelling. *Composites Part B: Engineering*, 311. <http://dx.doi.org/10.1016/j.compositesb.2025.113286>

N.B. When citing this work, cite the original published paper.



Electro-chemo-mechanical coupling in structural lithium-ion batteries: Experimental findings and numerical modelling

Rauan Al-Emrani *,¹, Carl Larsson ¹, Clara Dahlberg, Fredrik Larsson , Leif E. Asp , Johanna Xu *

Department of Industrial and Materials Science, Chalmers University of Technology, Gothenburg, SE-412 96, Sweden

ARTICLE INFO

Keywords:

Finite element analysis
Multiphysics modelling
Multifunctional materials
Carbon fibre composites

ABSTRACT

Structural batteries offer a promising route to reduce weight and volume in electrified systems by combining energy storage and mechanical functionality within a single composite material. However, understanding and quantifying the coupled electro-chemo-mechanical behaviour of such multifunctional materials remains a critical challenge, particularly at the level of full cell composites under mechanical load. Here, we present an integrated experimental–computational framework to capture voltage–strain coupling in laminated structural battery full cells composed of commercial lithium iron phosphate based positive electrodes, carbon fibre negative electrodes, and a phase separated structural battery electrolyte.

To interpret the experimental findings, we extend a continuum multiphysics model that captures the coupled chemo-mechanical behaviour of both electrodes, including a homogenised formulation for the lithium iron phosphate cathode. The model accurately reproduces the experimental potential shifts and identifies the carbon fibre electrode as the dominant contributor to the voltage–strain response. Notably, the weak coupling observed in the particle-based positive electrode provides critical insight into the electro-mechanical behaviour that can be expected in solid-state batteries employing similar cathode architectures. These findings offer a mechanistic understanding of stress–voltage interactions in structural battery systems and contribute to the broader knowledge base needed to advance structurally integrated energy storage technologies.

1. Introduction

Electrification represents a major trend in the transportation sector aimed at reducing greenhouse gas emissions. Over the past five years, this shift has significantly impacted the automotive industry, leading to the rapid adoption of electric passenger vehicles, such as cars and light goods vehicles. One of the greatest challenges in transport electrification is battery energy density. Current state-of-the-art lithium (Li)-ion batteries have an energy density of approximately 240 Wh/kg, vastly lower than petrol's 12,400 Wh/kg. This disparity means that a significantly larger mass of batteries is required to match the energy provided by a given mass of petrol. The increased vehicle mass then demands more energy to move, which in turn requires more batteries, creating a negative feedback loop.

A potential solution is to reduce overall vehicle weight by replacing monofunctional components with multifunctional material. Structural battery composites integrate load-bearing and energy storage functions,

offering weight and volume savings over separate structural and battery systems [1–7].

In the latest design, carbon fibres serve as the negative electrode and are coated with active lithium iron phosphate (LiFePO_4) to function as the positive electrode [8]. The electrodes, on each side of a separator are embedded in a phase-separated structural battery electrolyte (SBE). The solid part of the SBE is a polymeric phase in glassy state which adheres the constituents and thereby provides mechanical load transfer, while the liquid electrolyte phase contains a lithium salt solution which facilitates ionic conductivity.

The key difference between the state-of-the-art structural battery and previous designs lies in the choice of positive electrode, where previous structural battery designs used a LiFePO_4 (LFP) particle slurry adhered to an aluminium foil, instead of the carbon fibre based positive electrode [2,9–11]. Asp et al. demonstrated a laminated structural battery with intermediate modulus carbon fibres as negative electrode, a commercial LFP foil as positive electrode separated with a glass fibre

* Corresponding authors.

E-mail addresses: rauan@chalmers.se (R. Al-Emrani), calar@chalmers.se (C. Larsson), Fredrik.Larsson@chalmers.se (F. Larsson), leif.asp@chalmers.se (L.E. Asp), johanna.xu@chalmers.se (J. Xu).

¹ Authors contributed equally to this study.

weave, all impregnated with SBE by wet-layup [10]. This structural battery showed an energy density of 23 Wh/kg, an elastic modulus of 25 GPa and a tensile strength exceeding 300 MPa. Xu et al. showed that the capacity of the structural battery composite cells is only moderately affected by tensile loading up to 0.36% strain [12]. Improving the manufacturing technique by using a process similar to vacuum assisted resin transfer moulding, allowed for an increase in energy density to 42 Wh/kg, while maintaining the modulus [9].

In addition to energy and structural functionality, polyacrylonitrile (PAN) based carbon fibres exhibit a strong voltage-strain coupling effect when used as electrodes [13,14]. This coupling of mechanical and electrochemical responses through in-plane mechanical loading exemplifies the potential for innovative material solutions in the pursuit of strain-sensing composite materials. Moreover, the voltage-strain coupling also enables energy to be harvested from mechanical strains during lithiation/delithiation cycles [15]. Hence, it has previously been demonstrated that the electrochemical and mechanical properties influence each other in structural electrodes [16]. In conventional batteries, the coupling between mechanical stress and cell potential is also present, but is typically overlooked since the cells are not designed to bear mechanical loads. However in other research fields, such as flexible electronics, solid-state batteries, and electroactive actuators, this coupling is either a challenge to be mitigated or a feature to be exploited [17–22]. These examples demonstrate the broader relevance of understanding electro-chemo-mechanical interactions, emphasising the importance of this study in structural battery design. The electro-chemo-mechanical coupling is inherent to lithium insertion strains in the electrode materials [23]. For a structural battery this is of critical importance as high mechanical stresses will be inflicted on the lithiated carbon fibres.

Mechanical load applied on the carbon fibre electrode causes a shift in the electric potential that varies with the amount of Li that is inserted into the carbon fibres. Harnden et al. demonstrated a strain-sensing device using pre-lithiated carbon fibre bundles and a separator [24]. The sensor was later modelled by Carlstedt et al. where they resolve the carbon fibre electrodes on the microscale in 2D and upscale to a 1D beam problem in a FE² sense, and find good agreement between the voltage change in potential with the measured beam displacement and the computational prediction [25]. The electro-chemo-mechanical modelling methods proposed by Carlstedt et al. build on the theoretical foundation set by Newman and colleagues for conventional Li-ion batteries [25–29]. Duan et al. determined and compared the volume, and longitudinal and transverse moduli of a carbon fibre at pristine, fully lithiated and delithiated states [30]. Carbon fibres have been found to sustain high lithium insertion strains (approximately 1% in the axial and 7% in the radial direction) during electrochemical cycling [30]. Therefore, an immediate and strong electro-chemo-mechanical coupling effect is expected to result in the structural battery [16,23,25]. However, this coupling remains to be fully demonstrated and modelled (simulated) in mechanically functional structural battery systems.

Here we present a robust method for characterisation of the coupled voltage-strain effect for a laminated structural battery full cell with a commercial positive electrode, as illustrated in Fig. 1a. This method is used to demonstrate how the open circuit potential (OCP) responds to an external in-plane tensile load for cells, focusing on cells with low state of charge (SoC). To investigate the electro-chemo-mechanical response of structural battery laminates, full cells with LiFePO₄-coated commercial positive electrodes were subjected to combined electrochemical and mechanical cycling. Following initial electrochemical conditioning at a low charge rate (0.1 C, full charge/discharge in 10 h), the cells underwent five controlled mechanical loading cycles under displacement control. During loading, the open-circuit potential was continuously monitored via a potentiostat integrated with a microtester inside an inert atmosphere, revealing characteristic voltage–strain coupling (see Fig. 1b). To complement the experiments, we extend the multiphysics modelling framework developed by Larsson et al. enabling

predictive simulation of full cell behaviour under mechanical deformation [31]. The model incorporates coupling between electrochemical and mechanical fields within the LiFePO₄-based positive electrode, treating it as a homogenised continuum material. Effective electrode expansion is determined by upscaling particle-level behaviour based on the known volume fraction of active material. The influence of each electrode on the voltage-strain coupling effect is studied utilising the numerical model.

2. Materials and methods

2.1. Materials and cell manufacturing

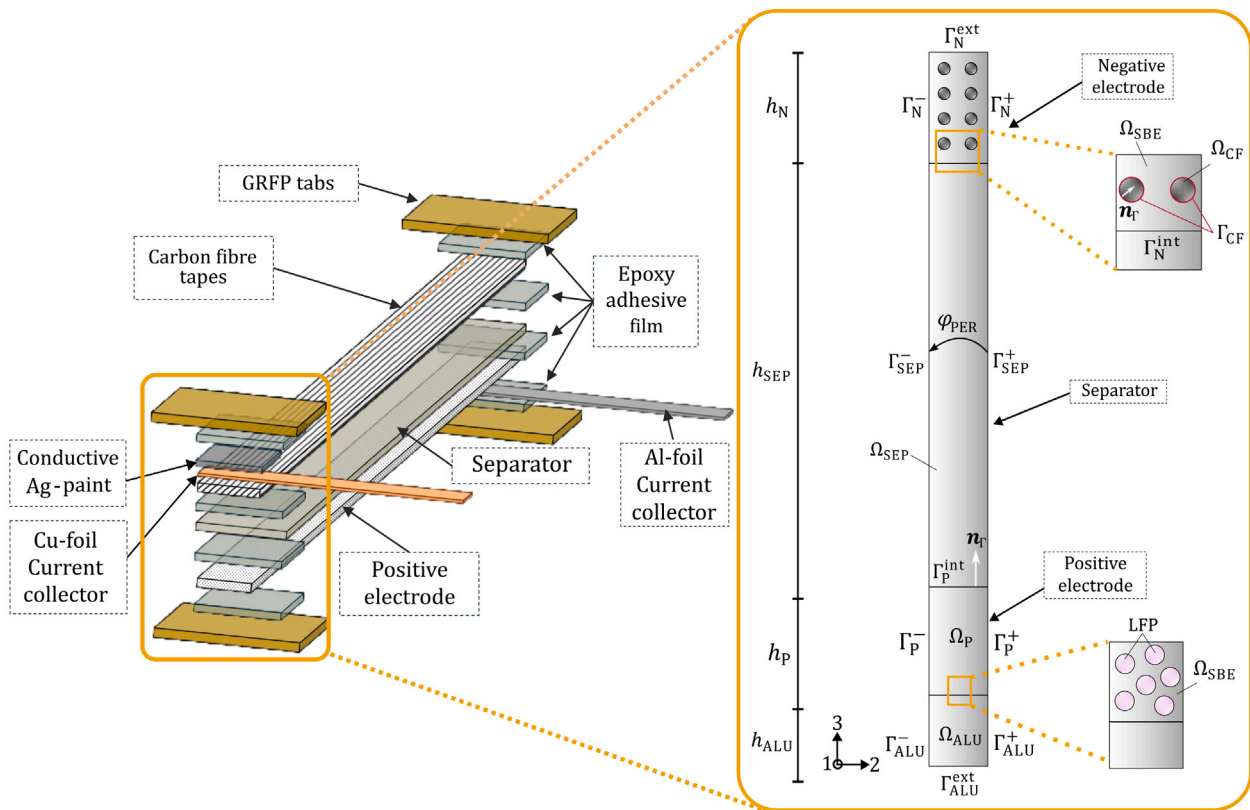
All cells were fabricated and pre-conditioned following established procedures validated in previous work [10,12], where both electrochemical and mechanical properties were shown to be highly reproducible. Asp et al. present an energy density of 11.6 Wh/kg and a specific power of 5.94 W/kg at 0.05 C for structural battery full cells with the same composition considered in the current experiments [10]. In the present study, representative full cell specimens were subjected to multiple electro-mechanical loading cycles to verify consistency of the voltage–strain response. The coupling behaviour was found to be stable and reversible across cycles, confirming the robustness of the measured effect.

For the negative electrode preparation, a single layer of unidirectional T800SC-12k-50C PAN-based carbon fibre tows (15 mm width, 0.52 g/m linear tow weight) supplied by Oxeon AB, Sweden, was split into approximately 5 mm wide tow. A copper foil strip current collector was adhered to the carbon fibres using silver conductive paint. A positive electrode, here, single sided coated LFP aluminium foil with active material loading density of 13 mg/cm² (purchased from MTI Corporation) was cut to match the dimensions of the carbon fibre electrode, and a strip of aluminium foil was used as current collector. A separator (Whatman glass-microfibre filter, Whatman GF/A, 260 μm thick, supplied by Sigma Aldrich) was placed between the two electrodes. To ensure proper gripping and load transfer during mechanical testing, 10 × 10 mm quasi-isotropic glass fibre composite tabs were adhered to the end of the specimens. Epoxy adhesive, DeltaPreg AX003 epoxy adhesive was used to adhere the tabs as well as materials between the tabs.

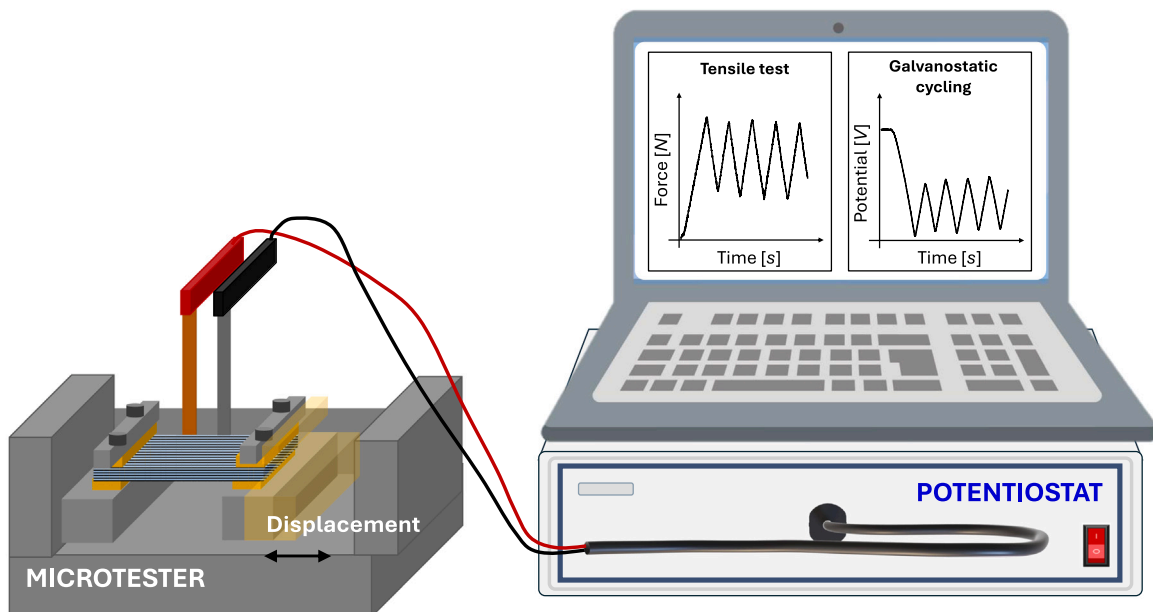
The two-phase bi-continuous SBE consist of a polymer material and a liquid electrolyte. Ethoxylated Bisphenol A dimethacrylate monomer (EBADMA) ($M_n = 540$ g/mol) was provided by Sartomer (Arkema Group). Thermal initiator 2,2'-azobis(2-methylpropionitrile) (AIBN), lithiumtrifluoromethanesulfonate (LiTf) and lithium bis(oxalato)-borate (LiBOB) salt, and organic solvents ethylene carbonate (EC) (battery grade, ≥99% acid < 10 ppm, H₂O < 10 ppm) and propylene carbonate (PC) (battery grade, ≥99% acid < 10 ppm, H₂O < 10 ppm) were purchased from Sigma Aldrich and used as received. The liquid electrolyte contains 0.6 M LiTf and 0.4 M LiBOB dissolved in EC and PC (50:50 wt %). The SBE solution is a mixture of liquid electrolyte, the monomer, and the thermal initiator.

During cell manufacturing, the tabbed dry layup was placed inside a pouch bag and infused with SBE via hand layup inside the glovebox. The SBE mixture was prepared in the glovebox in argon atmosphere (< ppm of H₂O, < 1 ppm of O₂), by mixing 50:50 wt % EBADMA and liquid electrolyte, and 1 wt % of monomer weight of AIBN thermal initiator. Following infusion, the pouch bag was vacuum sealed and thermally cured at 90 °C for 45 min.

Five low current density galvanostatic charge/discharge cycles were applied to precondition the structural battery cells. The applied current, corresponding to 0.1 C, was based on the theoretical C-rate calculated from the area capacity of the LFP-positive electrode (1 mAh cm⁻²). The cycling was carried out in a Neware CT-4008-5V10mA-164 battery cycler between 2.0 and 3.55 V. While the voltage limits for the structural battery define the nominal SoC range, the results are influenced by



(a)



(b)

Fig. 1. (a) Illustration of the dry layup of the structural battery sample for combined electro-chemo-mechanical characterisation. The zoom-in on the cross-section shows the geometry, domains and boundary conditions applied in the numerical model of the SBE-infused and cured full cell. (b) Schematic setup of the combined mechanical and electrochemical test.

high overpotentials inherent to the material system, which is a known challenge for structural batteries.

In the experiment, a cell with high SoC was prepared and the voltage-strain coupling effect was investigated in addition to two discharged cells. However, the cell with high SoC exhibited a large drop in potential as it was clamped into the tensile machine, which is believed to have occurred due to short-circuiting of the battery. Because of this uncertainty, the charged cell is not included in the presented results.

2.2. Experimental setup and voltage-strain coupling

The setup for combined mechanical and electrochemical testing was inside the glove box, with the current collectors connected to a potentiostat, Gamry Interface 1010E and the tabbed specimen mounted in the Deben UK micro-tensile tester, 2 kN tensile stage. The experimental setup is illustrated in Fig. 1b. The cells were mechanically loaded at a displacement rate of 0.2 mm/min.

It has previously been shown that carbon fibres activated using lithium ions exhibit a voltage-strain, or electro-chemo-mechanical coupling, known as the piezo-electrochemical transducer (PECT) effect [14]. This effect arises from mechanical strains caused by lithium insertion, altering the microstructure of the carbon fibres, and consequently, the chemical potential of the inserted ions. This alteration, in turn, changes the electrical potential of the cell [23,24]. This piezo-electrochemical effect, also known as voltage-strain coupling effect, is quantified by a coupling factor, relating the magnitude of the voltage change per unit change in strain. The coupling factor k is defined as

$$k = \frac{\Delta E}{\Delta \epsilon}, \quad (1)$$

where ΔE is the change in potential in the electrochemical cell and $\Delta \epsilon$, quantifies the mechanical strain. The coupling factor in Eq. (1), represents the relative change in open-circuit potential per unit strain. It provides insights into the voltage-strain coupling behaviour of structural battery materials under different experimental conditions, including displacement rates and mechanical loading and unloading.

The axial strain is calculated as

$$\epsilon = \frac{\Delta L}{L}, \quad (2)$$

where L is the specimen length and ΔL is the extension of the specimen obtained from the machine load.

2.3. Electro-chemo-mechanical modelling

Earlier work by Larsson et al. proposed a coupled electro-chemo-mechanical finite element model implemented in **COMSOL Multiphysics 6.2** using the *Weak form PDE* module [31]. Specifically, chemo-mechanical coupling is introduced on the electrodes, where the positive electrode is homogenised as a continuum, whereas the individual carbon fibres were resolved in the negative electrode. The Helmholtz free energy for the electrode domains is stated as

$$\psi(\epsilon, c_{Li}) = \frac{1}{2} \left[\epsilon - \alpha \frac{c_{Li} - c_{Li}^0}{\bar{c}} \right] : \mathbb{E}(c_{Li}) : \left[\epsilon - \alpha \frac{c_{Li} - c_{Li}^0}{\bar{c}} \right] + \bar{\psi}(c_{Li}, \bar{c} - c_{Li}), \quad (3)$$

applicable to the positive electrode domain P, or the carbon fibre domain CF. Furthermore, ϵ denotes the small strain tensor, c_{Li} is the concentration of lithium and c_v is the concentration of vacancies. The chemical part of the free energy is expressed as

$$\bar{\psi}(c_{Li}, c_v) = c_{Li} \mu_{Li}^0 + c_v \mu_v^0 + c_{Li} RT \ln(c_{Li}) + c_v RT \ln(c_v) + \Lambda(c_{Li}, c_v). \quad (4)$$

The elasticity tensor \mathbb{E} , the insertion induced (chemical) expansion tensor α , maximum concentration \bar{c} and concentration of vacant sites c_v are electrode specific quantities. We emphasise that the carbon fibre stiffness tensor, \mathbb{E}_{CF} and corresponding expansion tensor α_{CF} , is

anisotropic, whereas the stiffness tensor of the particle, \mathbb{E}_P and expansion tensor α_P , is isotropic. The connection between the maximum and vacant site concentrations is expressed as $\bar{c} = c_{Li} + c_v$. Furthermore, $\Lambda(c_{Li}, c_v)$ is a function describing the deviation from ideal conditions, related to the interaction of the vacant sites and lithium species. μ_{Li}^0 and μ_v^0 denotes the reference chemical potentials for the Li species and vacancies, R is the ideal gas constant and T is the temperature. Based on the free energy formulation, the following constitutive relations for mechanical stress σ , and chemical potential μ_{Li}^{en} , can be expressed as

$$\sigma(\epsilon, c_{Li}) = \frac{\partial \psi}{\partial \epsilon} = \mathbb{E}(c_{Li}) : \left[\epsilon - \alpha \frac{c_{Li} - c_{Li}^0}{\bar{c}} \right], \quad (5a)$$

$$\begin{aligned} \mu_{Li}^{en}(\epsilon, c_{Li}) &= \frac{\partial \psi}{\partial c_{Li}} = -\frac{1}{\bar{c}} \alpha : \sigma + \mu^0 + RT \ln\left(\frac{c_{Li}}{\bar{c} - c_{Li}}\right) + \frac{d}{dc_{Li}} \Lambda(c_{Li}, \bar{c} - c_{Li}) \\ &\quad + \frac{1}{2} \sigma : [\mathbb{E}(c_{Li})]^{-1} : \frac{\partial \mathbb{E}(c_{Li})}{\partial c_{Li}} : [\mathbb{E}(c_{Li})]^{-1} : \sigma. \end{aligned} \quad (5b)$$

We note the coupled terms $-\mathbb{E}(c_{Li}) : \alpha \frac{c_{Li} - c_{Li}^0}{\bar{c}}$ in Eq. (5a) contain the contribution of lithium concentration to mechanical stress, and $-\frac{1}{\bar{c}} \alpha : \sigma + \frac{1}{2} \sigma : [\mathbb{E}(c_{Li})]^{-1} : \frac{\partial \mathbb{E}(c_{Li})}{\partial c_{Li}} : [\mathbb{E}(c_{Li})]^{-1} : \sigma$ in Eq. (5b) contains the influence of mechanical stress and concentration dependent stiffness on the chemical potential.

The aforementioned constitutive equations are utilised for solving the boundary value problem consisting of three PDE's solved over the different domains $\Omega = \Omega_{CF} \cup \Omega_{SBE} \cup \Omega_{SEP} \cup \Omega_P \cup \Omega_{ALU}$ shown in Fig. 1. The mechanical problem (quasi-static) is solved over the all the domains where periodic boundary conditions are applied on the vertical boundary $\Gamma^+ = \Gamma_{ALU}^+ \cup \Gamma_P^+ \cup \Gamma_{SEP}^+ \cup \Gamma_N^+$ mirrored to its counterpart on Γ^- . The mechanical problem is stated as:

$$-\sigma \cdot \bar{\nabla} = \mathbf{0} \quad \text{in } \Omega, \quad (6)$$

$$\bar{u}^+ - \bar{u}^- = \mathbf{0}, [\sigma^+ - \sigma^-] \cdot \mathbf{n}^+ = \mathbf{0} \quad \text{on } \Gamma^+, \quad (7)$$

$$\sigma \cdot \mathbf{n} = \mathbf{0} \quad \text{on } \Gamma_N^{\text{ext}} \cup \Gamma_{ALU}^{\text{ext}}, \quad (8)$$

where \bar{u} is the displacement field in the transverse plane, \mathbf{n} is the unit normal pointing outwards and $\bar{\nabla}$ is the differential operator pertinent to the transverse plane. We consider all interfaces to be perfectly elastic. Furthermore, we utilise generalised plane strain for the structure and divide the mechanical problem into transversal and fibre-direction components. The fibre direction aligns with the basis vector e_1 and the transverse plane is associated with the basis vectors e_2 and e_3 . Thereby, the strain tensor can be constructed as

$$\epsilon = \bar{\epsilon}(\bar{u}) + \bar{\epsilon} e_1 \otimes e_1, \quad (9)$$

where $\bar{\epsilon}$ is the (uniform) strain component in the fibre direction. The complementary equation that is added to determine the strain component is expressed as

$$\int_{\Omega} \sigma_{11} d\Omega - F_{\text{app}} = 0, \quad (10)$$

where F_{app} is the applied force obtained from the conducted experiments.

The electro-chemical problem for transport of lithium ions and the related anion denoted X is stated below:

$$\dot{c}_\alpha + j_\alpha \cdot \bar{\nabla} = 0 \quad \text{in } \Omega_{SEP} \cup \Omega_{SBE}, \quad \alpha = Li, X, \quad (11)$$

$$F[c_{Li} - c_X] - \mathbf{d} \cdot \bar{\nabla} = 0 \quad \text{in } \Omega_{SEP} \cup \Omega_{SBE}, \quad (12)$$

$$\mu_\alpha^+ - \mu_\alpha^- = 0, [j_\alpha^+ - j_\alpha^-] \cdot \mathbf{n}^+ = 0 \quad \text{on } \Gamma_{SEP}^+ \cup \Gamma_N^+, \quad \alpha = Li, X, \quad (13)$$

$$\varphi^+ - \varphi^- = 0, [\mathbf{d}^+ - \mathbf{d}^-] \cdot \mathbf{n}^+ = 0 \quad \text{on } \Gamma_{SEP}^+ \cup \Gamma_N^+, \quad (14)$$

$$j_{Li} \cdot \mathbf{n} = -j_P, \mathbf{d} \cdot \mathbf{n} = -d_P \quad \text{on } \Gamma_P^{\text{int}}, \quad (15)$$

$$j_{Li} \cdot \mathbf{n} = j_N, \mathbf{d} \cdot \mathbf{n} = d_N, \quad \text{on } \Gamma_{CF}, \quad (16)$$

$$j_{Li} \cdot n = 0, d \cdot n = 0 \quad \text{on} \quad \Gamma_N^{\text{ext}}, \quad (17)$$

$$j_X \cdot n = 0 \quad \text{on} \quad \Gamma_P^{\text{int}} \cup \Gamma_N^{\text{ext}} \cup \Gamma_{CF}. \quad (18)$$

Here, the primary field variables are the chemical potential μ_α of the two species and the electric potential φ . The chemical problem is solved from the mass-balance stated in Eq. (11) and the electrical potential is obtained from Eq. (12). The concentration c_α and ionic flux j_α of the two species are determined from constitutive relations as functions of the chemical potential as well as electric potential. Furthermore, periodicity is enforced, again on the vertical boundaries $\Gamma_{SEP}^+ \cup \Gamma_N^+$ mirrored to its counterpart. Finally, we solve the chemical problem inside the electrodes, governed by mass conservation of neutral lithium atoms as

$$\dot{c}_{Li} + j_{Li} \cdot \bar{\nabla} = 0 \quad \text{in} \quad \Omega_P \cup \Omega_{CF}, \quad (19)$$

$$\mu_{Li}^+ - \mu_{Li}^- = 0, [j_{Li}^+ - j_{Li}^-] \cdot n^+ = 0 \quad \text{on} \quad \Gamma_P^+, \quad (20)$$

$$j_{Li} \cdot n = j_P \quad \text{on} \quad \Gamma_P^{\text{int}}, \quad (21)$$

$$j_{Li} \cdot n = -j_N \quad \text{on} \quad \Gamma_{CF}, \quad (22)$$

$$j_{Li} \cdot n = 0 \quad \text{on} \quad \Gamma_P^{\text{ext}}. \quad (23)$$

Again, the primary variable we choose from Eq. (19) is the chemical potential inside the electrodes. Similarly to the electrolyte domain, constitutive relations are introduced for the flux j_{Li} and concentration c_{Li} as functions of the chemical potential. The neutral lithium atoms are not affected by the local electric field and therefore no electro-chemical coupling is needed for the electrode domains. However, the chemo-mechanical coupling is introduced on the electrodes. Along with the constitutive relations shown in Eqs. (5a) and (5b), the system (11)–(23) governs the effective coupling between applied force and electric potential shown in the results. The interface fluxes $j_{P/N}$ and $d_{P/N}$ are chosen as Butler-Volmer type in accordance with [31].

2.4. Estimation of material parameters

Here, two modifications to the model presented by Larsson et al. are proposed [31]. Firstly, the chemo-mechanical properties of the homogenised positive electrode are calculated. Secondly, mechanical properties of the separator domain and the aluminium foil used as current collector are introduced. The domains in the modified numerical model are schematically illustrated in Fig. 1a and the modifications are described as follows.

Chemo-mechanical properties of the positive electrode domain (Ω_P) concern its homogenised elastic and expansion properties. These properties relate to the amount of LFP and SBE in the electrode assuming iso-stress conditions (i.e., Reuss assumption) as

$$\mathbb{E}_P = (\mathbb{E}_{LFP}^{-1} V_{LFP}^f + \mathbb{E}_{SBE}^{-1} (1 - V_{LFP}^f))^{-1}, \quad (24)$$

where \mathbb{E}_P denotes the elasticity tensor of the homogenised positive electrode. It should be noted that the positive electrode slurry consists of 95.4% LFP. The influence of the remaining 2% PVDF and 2.6% Super P carbon black is neglected. The elasticity tensors \mathbb{E}_{LFP} and \mathbb{E}_{SBE} are defined for the LFP particles and the SBE, respectively. Qi et al. reported a Young's modulus for the isotropic LFP of 124 GPa [32]. Similarly, Tavano et al. reported an elastic modulus of the isotropic SBE, E_{SBE} , to be 412 MPa [33]. The volume fraction of LFP particles in the positive electrode, V_{LFP}^f , is set to 55%. The following elastic properties for the homogenised positive electrode resulted; a Young's modulus of 0.22 GPa and a Poisson's ratio of 0.34. The calculated Young's modulus is close to that measured for a commercial NMC positive electrode by Gupta et al. [34].

The same approach is used to estimate the expansion coefficient. Thus, the expansion coefficient is expressed as

$$\bar{\alpha}_P = \alpha_{LFP} V_{LFP}^f. \quad (25)$$

Here, an isotropic expansion coefficient, α_{LFP} , of 6.77% reported by Zhang et al. is used [35]. For a volume fraction of LFP of 55% an expansion coefficient for the homogenised positive electrode domain of 3.7% results. The mechanical properties of the full cell are calculated following the introduction of the aluminium domain. The 16 μm thick aluminium current collector has an elastic modulus of 70 GPa.

The elastic properties of the homogenised separator domain are calculated based on the known properties of the other domains. The longitudinal elastic modulus of the negative electrode domain is calculated by the rule of mixtures following the iso-strain, Voigt assumption as

$$E_L^N = V_{CF}^f E_L^{CF} + (1 - V_{CF}^f) E_{SBE}. \quad (26)$$

Asp et al. reported a carbon fibre volume fraction, V_{CF}^f , of 20% for the type of structural battery full cell with a commercial positive electrode studied here [10]. The longitudinal elastic modulus of the T800 carbon fibres, E_L^{CF} , is 294 GPa [36]. Hence, the resulting longitudinal elastic modulus, E_L^N , and major Poisson's ratio, ν_{LT}^N , are 59.1 GPa and 0.32, respectively.

The homogenised elastic modulus of the separator domain is calculated as

$$\bar{E}_{SEP} = \frac{E_L h_{tot} - E_L^N h_N - E_P h_P - E_{ALU} h_{ALU}}{h_{SEP}}. \quad (27)$$

The domains and the geometry in the numerical model are defined according to Fig. 1a. The thickness of the negative electrode domain (50 μm) and separator domain (260 μm) are the same as those used in the previous model by Larsson et al. [31]. In contrast, a thickness of the homogenised LFP slurry and aluminium foil of 68 μm and 16 μm , respectively, are used in the current model. However, when calculating the homogenised elastic modulus of the separator domain, the thickness of the negative electrode is set to 65 μm , based on the work presented by Asp et al. where the average longitudinal elastic modulus, E_L , is 18.3 GPa [10]. With this input an elastic modulus of the homogenised separator domain of 9.6 GPa results. Furthermore, using the modified rule of mixtures for short fibre composites a Poisson's ratio of 0.49 is achieved for the homogenised separator domain with a glass fibre volume fraction of 34%.

3. Results and discussion

3.1. Voltage-strain coupling factor from experiments

The first mechanical loading cycle was excluded due to initial artifacts such as fibre straightening. Coupling factors were extracted from the second through fifth cycles using the relations detailed in Section 2.2 (Eqs. (1) and (2)), yielding values of 0.86 (loading) and 0.85 (unloading) at low state of charge. This symmetry indicates a stable and reversible coupling effect under quasi-static loading conditions. Jacques et al. reported coupling factors exceeding 1 for delithiated carbon fibres in half-cells with liquid electrolyte, peaking at 1.5 around 50% SoC and declining to 1.3 when fully lithiated [14]. Harnden et al. observed comparable trends for potassium- and sodium-ion systems [37].

Although the voltage-strain coupling factor for the delithiated fibres measured here is slightly lower than Jacques's results, the values are within reasonable limits. The discrepancy can be explained by several factors. Jacques et al. conducted tests on carbon fibres in liquid electrolyte, whereas the tests reported here were performed in SBE. This procedural difference likely contributes to the variation in the measured coupling factor, as the amount of Li inserted in the carbon fibres may differ. Carlstedt et al. previously showed that a certain knock-down in electrochemical capacity exists for carbon fibres cycled in SBE versus liquid electrolyte [38]. The use of liquid electrolyte also requires a protective sealant, meaning the cell clamped into the tensile tester was still in the pouch bag in Jacques's and Harnden's experiments. In contrast, our cell configuration, the battery full cell with added

tabbing material was clamped into the tensile machine, no pouch bag was used. This distinction likely contributes to the difference in the measured coupling factor as well. Another key difference compared to previous half-cell studies is the potential contribution of the LFP positive electrode to the PECT effect. Here, this effect is quantified in the homogenised LFP electrode, providing important insight for strain-sensing functionality in structural battery full cells.

3.2. Validation of the elastic modulus in the fibre direction

The mechanical properties of the homogenised positive electrode and the separator domain were estimated using homogenisation techniques, it is therefore necessary to validate the stiffness of the full cell predicted by the numerical model. Assuming generalised plane strain and only considering mechanical analysis, the homogenised stress in the fibre direction, $\bar{\sigma}_{11}$, is post-processed according to

$$\bar{\sigma}_{11} = \frac{1}{|\Omega|} \int_{\Omega} \sigma_{11} d\Omega, \quad (28)$$

where σ_{11} represents the stress component parallel to the fibre direction. Upon calculating the homogenised longitudinal stress, $\bar{\sigma}_{11}$, from Eq. (28) and the corresponding strain component with Eqs. (9) and (10), the elastic modulus in the longitudinal direction is calculated to be 19.0 GPa. In comparison, Asp et al. reported an elastic modulus of 18.3 GPa for similar cells measured in tensile tests parallel to the carbon fibres [10]. The close agreement validates the material properties and geometric assumptions used in the model, confirming that the implementation accurately captures the mechanical stiffness of the structural battery full cells tested experimentally.

3.3. Lithium concentration in the negative electrode as function of state of charge

To predict the electro-chemo-mechanical coupling effect under prescribed displacement, it is necessary to estimate the relative concentration in both electrodes during electrochemical cycling. Here, the numerical model is used to determine how the relative lithium concentration varies in the electrode domains during cycling. The model is based on calibrated data from previous experiments conducted on different cells to the ones presented here. The non-linear, fully coupled, electro-chemo-mechanical problem, as detailed in Section 2.3, is solved using the finite element method. The strongly non-linear problem requires fine spatial and temporal discretisation. The lithium concentration in the fibres changes with the state of charge, and is at its minimum when the cell is discharged. In the experiments the cells were cycled between 3.55 V at charge and 2 V at discharge, for a charge rate of 0.1 C. Hence, through utilisation of the numerical model, a full galvanostatic charge/discharge cycle at 0.1 C is simulated, as illustrated in Fig. 2a. Fig. 2b shows the calculated voltage profile, Φ^+ , that appears due to galvanostatic cycling. The simulation starts from a fully discharged state and is rested for approximately an hour at full state of charge, and thereafter it is discharged.

To calculate how the relative concentration varies with time, we assume that the initial relative concentration in the carbon fibres (at $t = 0$ s) is 1%, as depicted in Fig. 2c. The initial lithium concentration in the homogenised positive electrode is estimated according to Fig. 2d, where the volume of the electrode domains is considered with the following condition

$$V_{CF}c_{CF}^0 + V_Pc_P^0 = \bar{c}_{tot} \leq V_P\bar{c}_P. \quad (29)$$

Here, V_{CF} describes the total volume of the fibres and V_P is the volume of the homogenised positive electrode. The total lithium concentration in the electrode domains is given by \bar{c}_{tot} , which has to be less than, or equivalent to the product between the maximum lithium concentration and the volume of the positive electrode domain, where $\bar{c}_P = 10,373$ mol/m³ as presented by Larsson et al. [31]. Since the initial lithium

concentration in the carbon fibres, c_{CF}^0 , is known from the initial relative lithium concentration in the fibres ($c_{CF}^0 = 0.01\bar{c}_{CF}^0$), the initial lithium concentration in the homogenised positive electrode, c_P^0 , can be calculated with Eq. (29) considering that $\bar{c}_{tot} = V_P\bar{c}_P$. To obtain the relative concentration in both electrodes during the full charge/discharge cycle, it is necessary to homogenise the lithium concentration in the active electrode materials according to

$$\bar{c}_{CF/P} = \frac{1}{|\Omega_{CF/P}|} \int_{\Omega_{CF/P}} c_{Li} d\Omega, \quad (30)$$

where c_{Li} is the lithium concentration in the active electrode materials. Thereafter, the relative concentration is calculated scaling the homogenised lithium concentration in Eq. (30), $\bar{c}_{CF/P}$, over the maximum lithium concentration for the active electrode materials, \bar{c} . From Larsson et al. the maximum lithium concentration in the carbon fibres is calibrated to $\bar{c}_{CF} = 15,609$ mol/m³ [31]. At $t = 9.7$ h, the cell is fully charged and the relative lithium concentration in the carbon fibres is 60% of the maximum concentration, as shown in Fig. 2c. After the cell has been rested for 58 min, it is discharged and at 2 V the relative lithium concentration is estimated to 0.3%. This value differs from the assumed 1% initial concentration at $t = 0$ h for the given charge rate of 0.1 C. The predicted lithium ion concentration in the discharged cell is used in the analysis of the electro-chemo-mechanical model.

3.4. The electro-chemo-mechanical coupling in the cell is dominated by the carbon fibre electrode

To assess how the electrodes influence the variation of the open cell potential during mechanical loading, the contribution of the electro-chemo-mechanical coupling effect from each electrode domain was isolated in the numerical model. This is studied for the discharged cell mechanically loaded with a 0.2 mm/min displacement rate, disregarding the coupled terms in Eqs. (5a) and (5b) for each electrode, separately. First, electro-chemo-mechanical coupling is considered only for the negative electrode, where the expansion coefficient in the longitudinal and transverse direction of the carbon fibre is $\alpha_L = 0.0085$ and $\alpha_T = 0.066$, respectively [30,38]. Similarly, when electro-chemo-mechanical coupling is solely considered for the positive electrode, the coupling terms are excluded for the negative electrode. The expansion coefficient for the homogenised positive electrode domain, $\bar{\alpha}_P$, was calculated to 0.037 in accordance with Eq. (25), and is considered as isotropic. Finally, coupling was applied to both electrodes simultaneously.

Fig. 3 shows how the normalised potential, $\bar{\Phi}(t) = \frac{\Phi(t)}{\Phi(0)}$, (the values are normalised with the initial potential) changes over time for different implementations of electro-chemo-mechanical coupling. When coupling is considered on both electrodes, the response is similar to the experiment, with marginal differences in potential range. In comparison, when the coupling terms are only considered for the negative electrode, the cyclic variation of the potential is almost identical to when electro-chemo-mechanical coupling is considered for both electrodes. However, when coupling is only considered for the positive electrode, the potential is almost constant, which deviates from the experiments. From Fig. 3, it can also be noted that the amplitude in potential is orders of magnitude more sensitive to applied mechanical loading when voltage-strain coupling is considered for the negative electrode versus the positive electrode. These results demonstrate that the carbon fibres in the negative electrode govern the electro-chemo-mechanical coupling in structural battery full cells with a commercial positive electrode.

In the experiment, two discharged cells were mechanically loaded at a 0.2 mm/min displacement rate, where the applied force for the first cell is presented in Fig. 4a. For the second cell, a 60 s hold at maximum and minimum displacement was included for each load cycle, as shown in Fig. 4b. Figs. 4c-4f compare how the open cell potential changes with applied mechanical load in the experiment and

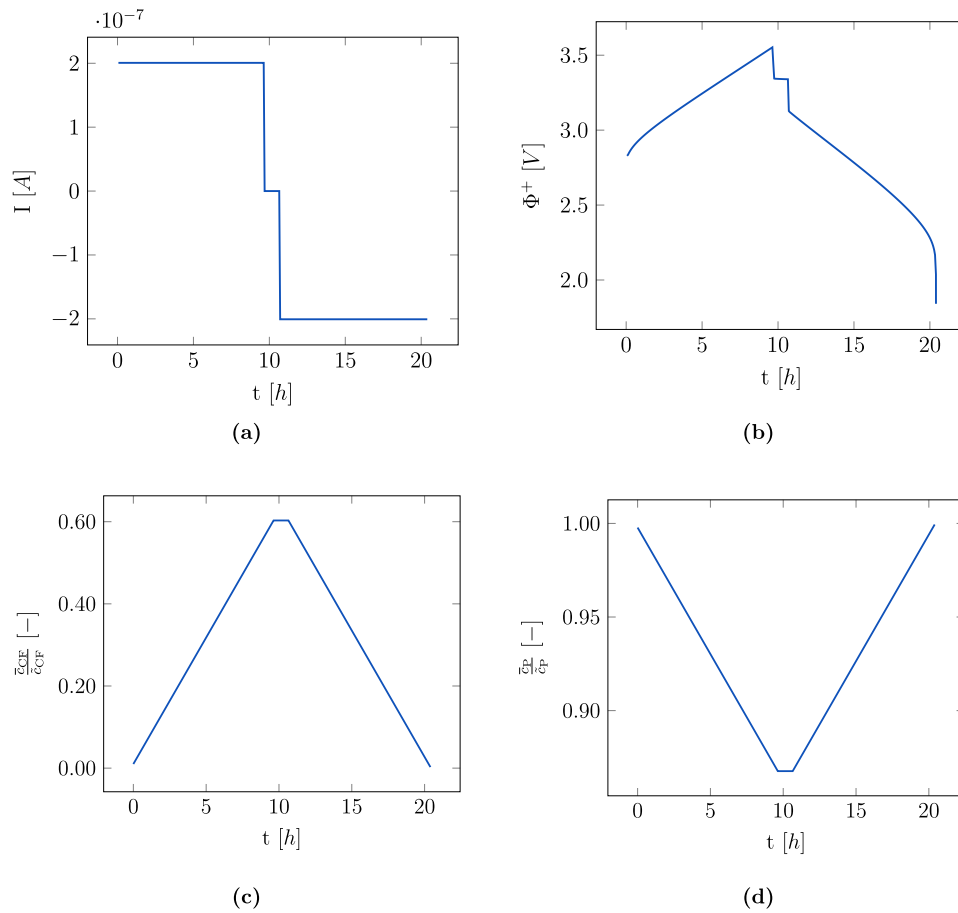


Fig. 2. Cell cycling at 0.1 C simulated for (a) the current (I) (b) the calculated potential (Φ^+) (c) the relative lithium concentration in the carbon fibres ($\frac{\bar{c}_{CF}}{c_{CF}^0}$) (d) the relative lithium concentration in the positive electrode ($\frac{\bar{c}_p}{c_p^0}$).

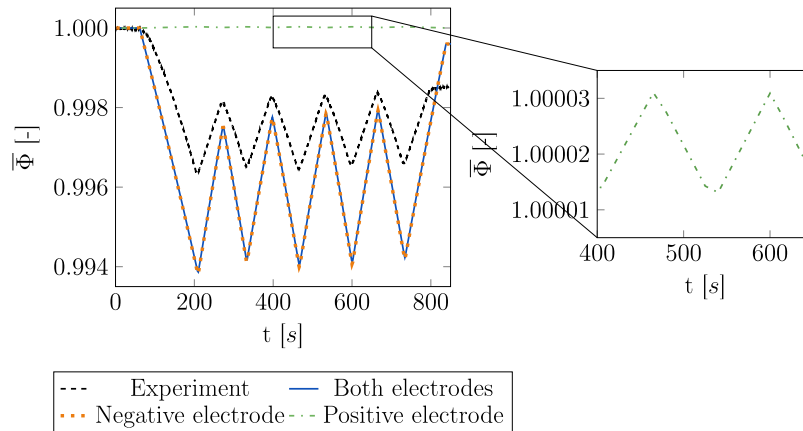


Fig. 3. The calculated electric potential-time curve of the delithiated cell during mechanical loading at 0.2 mm/min displacement rate, when electro-chemo-mechanical coupling is considered for both electrodes compared to each electrode separately. The potential is normalised ($\bar{\Phi}$) and the results are compared to the corresponding experiment. It is seen that the contribution from the positive electrode is negligible for structural battery full cells with a commercial positive electrode. The OCP of the full cell is orders of magnitude less sensitive to mechanical loading when coupling is only considered for the positive electrode, as seen by the zoomed inset.

in model predictions. The first cell shows a maximum difference of 0.23 V between the experiment and the numerical results, as presented in Fig. 4c. In contrast, the maximum difference in potential for the second cell with a 60 s hold between mechanical load ramps, is 0.21 V as shown in Fig. 4e. Figs. 4d and 4f present the normalised potential for the first and second cells, respectively. It is shown that the numerical

model predicts slightly wider amplitude ranges in potential for each cycle compared to the experiments. Despite the marginal differences, the numerical model is able to accurately predict the cyclic behaviour of the potential during the tensile test for the discharged cells.

In addition to presented results, the homogenised strain parallel to the fibres, $\bar{\epsilon}_{11}$, that occurs due to mechanical loading, is calculated

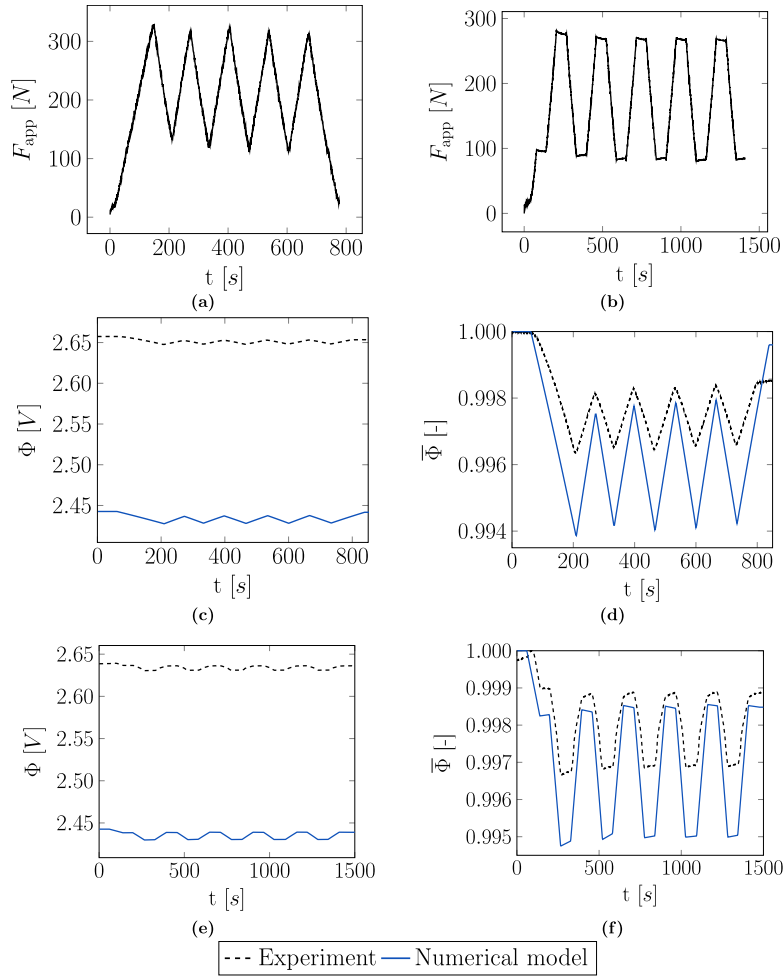


Fig. 4. Applied force, F_{app} , during the experiment at a displacement rate of 0.2 mm/min on (a) the first cell (b) the second cell. The OCP response is measured over time during mechanical loading and compared to the numerical model for (c) the obtained potential, Φ , of the first cell (d) normalised potential, $\bar{\Phi}$, of the first cell (e) the obtained potential, Φ , of the second cell (f) normalised potential, $\bar{\Phi}$, of the second cell.

using the numerical model. Furthermore, during the experiments, the two cells were mechanically loaded at a 0.5 mm/min displacement rate. These load cases were also simulated, and the result was compared to the potential obtained in the experiment. The additional results are presented in Supplementary information.

3.5. Sensitivity of voltage response to lithium concentration and expansion coefficient

Since the carbon fibres in the negative electrode dominate the electro-chemo-mechanical behaviour of the full cell, a sensitivity analysis related to the lithium concentration in the fibres is conducted. Changing the initial lithium concentration and the longitudinal expansion coefficient in α influence the coupling terms $-\mathbb{E}(c_{Li}) : \alpha \frac{c_{Li} - c_{Li}^0}{\bar{c}}$ in Eq. (5a) and $\frac{1}{2} \sigma : [\mathbb{E}(c_{Li})]^{-1} : \frac{\partial \mathbb{E}(c_{Li})}{\partial c_{Li}} : [\mathbb{E}(c_{Li})]^{-1} : \sigma$.

We note that the base-line potential, Φ , is governed by the chemical potential $\mu_{Li}^{en}(\epsilon, c_{Li})$ in Eq. (5b). For the case of zero stress ($\sigma = \mathbf{0}$) we obtain $\epsilon = \alpha \frac{c_{Li} - c_{Li}^0}{\bar{c}}$, in turn the chemical potential can be expressed as

$$\mu_{Li}^{en}(c_{Li}) \Big|_{\sigma=0} = \mu^0 + RT \ln \left(\frac{c_{Li}}{\bar{c} - c_{Li}} \right) + \frac{d}{dc_{Li}} \Lambda(c_{Li}, \bar{c} - c_{Li}), \quad (31)$$

unaffected by α and exhibit no coupling.

If the electrode is loaded faster than the characteristic lithium diffusion time, we can assume a fixed (homogeneous) lithium concentration c_{Li} , while the mechanical stress is given by loading ($\sigma \neq \mathbf{0}$). In this

setting, the sensitivity of the chemical potential to mechanical stress can be expressed as

$$\Delta \mu_{Li}^{en}(\epsilon, c_{Li}) \Big|_{\sigma \neq 0} = \Delta \left(-\frac{\alpha}{\bar{c}} : \sigma + \frac{1}{2} \sigma : [\mathbb{E}(c_{Li})]^{-1} : \frac{\partial \mathbb{E}(c_{Li})}{\partial c_{Li}} : [\mathbb{E}(c_{Li})]^{-1} : \sigma \right). \quad (32)$$

Clearly, the chemical potential is primarily affected by the magnitude of α , and influenced by the contribution from the concentration dependent stiffness.

A variation in the initial lithium concentration in the carbon fibres for the discharged cell is studied as shown in Fig. 5a. The lithium concentration in the carbon fibres is defined as the product between the relative concentration, and the maximum lithium concentration in the carbon fibres, \bar{c}_{CF} . The study includes the initial implementation, where the relative concentration in the fibres at discharge is calculated to 0.3%. Therefore, the initial lithium concentration in the carbon fibres is $c_{CF}^0 = 0.003\bar{c}_{CF}$. If the initial lithium concentration (c_{Li}^0 in Eq. (5a)) is decreased to $0.001\bar{c}_{CF}$, the potential decreases compared to the baseline case, thus increasing the gap between predicted and measured potential. However, the amplitudes in potential remains unchanged from the initial implementation. Increasing the carbon fibre concentration to $0.009\bar{c}_{CF}$, the opposite effect is observed, and the potential increases to values close to those measured in the experiment. Thus, an increase in the initial lithium concentration of the carbon fibres increases the potential, while the amplitude in potential remains constant.

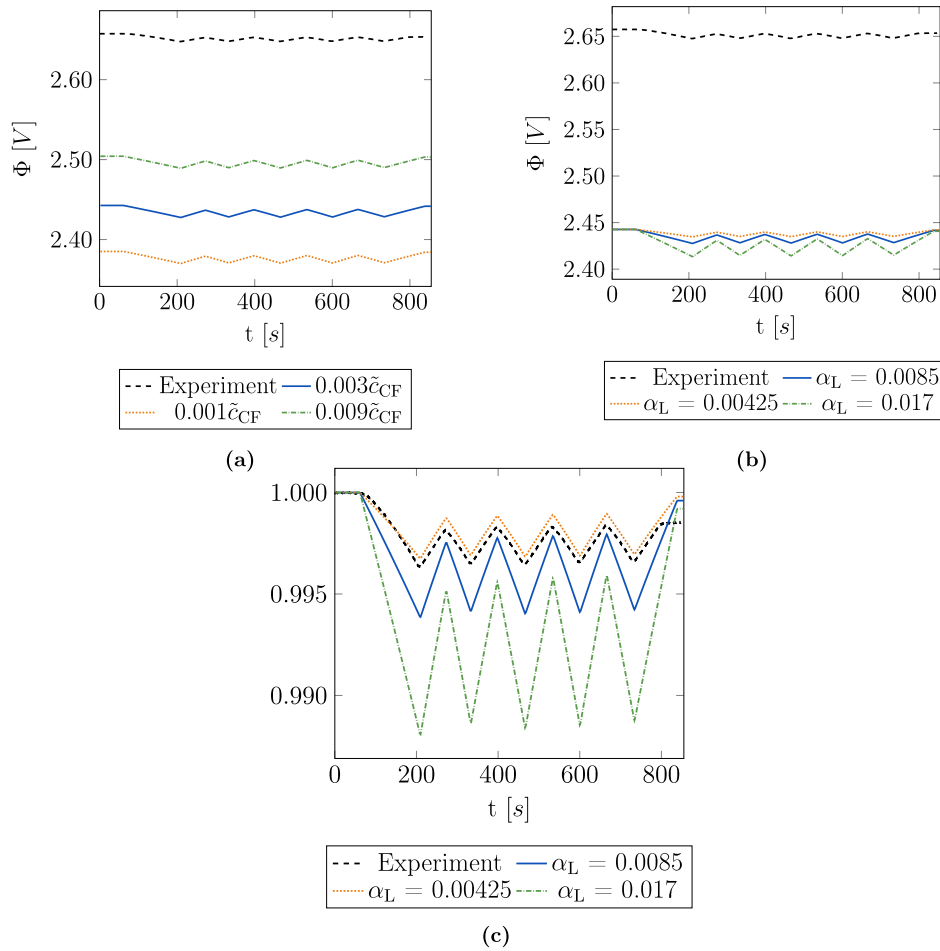


Fig. 5. Sensitivity of the potential when changing the (a) initial lithium concentration and (b) the longitudinal expansion coefficient. Additionally, (c) shows the normalised potential when changing the longitudinal expansion coefficient.

Fig. 5b shows how the potential changes when the longitudinal expansion coefficient, α_L , included in the expansion tensor for the carbon fibres, α , in Eqs. (5a) and (5b) is varied. In the initial simulation, $\alpha_L = 0.0085$ was used, in accordance to previously measured data for T800 carbon fibres in liquid electrolyte [38]. When reduced by 50%, the initial potential is unchanged, however the amplitude of the potential is decreased due to the reduced coupling effect. When the longitudinal expansion coefficient is increased to 0.017, the range in potential increases. In comparison to the experiment, the normalised result in **Fig. 5c** shows that a reduced longitudinal expansion coefficient results in electric potential amplitudes closer to the experimental results.

3.6. Parameter calibration

To quantitatively match the experimental voltage–strain response, we identify two key parameters that govern the electro-chemo-mechanical behaviour of the structural battery cell; the initial lithium concentration in the carbon fibres and the longitudinal chemical expansion coefficient. Sensitivity analyses presented in **Fig. 5**, show that the initial baseline potential is primarily determined by the initial lithium concentration, while the electrical potential variation under mechanical load is controlled by the longitudinal expansion coefficient of the carbon fibres. Based on these observations, we calibrate the model using least-squares optimisation to minimise the discrepancy between

simulated and measured potentials over time according to

$$\theta^* = \arg \min_{\theta} \sum_{n=1}^N (\Phi^+(\theta, t_n) - \Phi_{\text{exp}}(t_n))^2, \quad (33)$$

where Φ^+ and Φ_{exp} denote the simulated and experimental potentials at time step t_n , and $\theta = [c_{CF}^0 \quad \alpha_L]$ represents the calibrated parameters. The optimised parameter set, **Fig. 6a**, with an initial lithium concentration in the carbon fibre domain of 982 mol/m^3 (corresponding to 6.3% of the maximum) and a longitudinal expansion coefficient for the carbon fibres of 0.0051, produces close agreement with the experimental data. In comparison, Carlstedt et al. report that the longitudinal expansion coefficient for carbon fibres in SBE is 0.006, hence validating the calibrated result [38]. Additionally, the voltage fluctuations induced by mechanical loading are accurately reproduced by the model, **Fig. 6b**, confirming the predictive capability of the coupled simulation framework.

4. Conclusions

This work establishes a comprehensive and experimentally validated framework for quantifying electro-chemo-mechanical coupling in structural battery full cells, demonstrating both methodological rigor and novel predictive capabilities. Through tensile testing of LiFePO_4 -based full cells at low state-of-charge, we reveal a stable and reversible voltage–strain response that directly evidences electro-chemo-mechanical coupling under mechanical load, extending observations

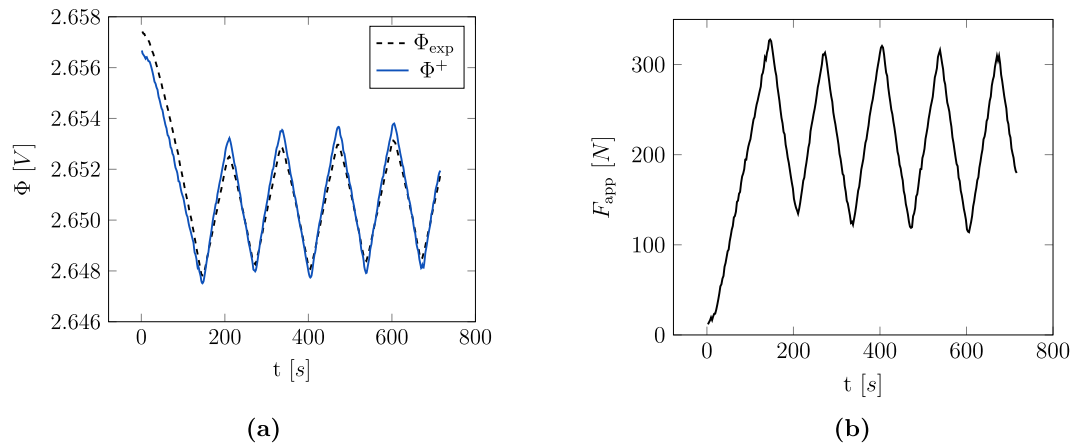


Fig. 6. (a) Experimental and simulated cell potential with optimised parameters profiles. (b) Applied force profile causing the variation in cell potential in (a).

previously limited to half-cells or liquid electrolyte systems. This is the first demonstration of such coupling in structurally integrated, mechanically loaded full cell laminates employing a phase-separated structural battery electrolyte.

Notably, we extend a multiphysics continuum model to incorporate chemo-mechanical coupling in both electrodes, including the homogenised LiFePO_4 cathode, an advance over previous models that often resolved only the negative electrode. The model accounts for lithium concentration-dependent expansion and mechanical stress effects, enabling quantitative simulation of full cell voltage response under in-plane deformation. Validation against experimental measurements confirms that the carbon fibre negative electrode dominates the electro-mechanical response, while sensitivity analyses identify key governing parameters such as initial lithium content and axial expansion coefficients. The limited coupling observed in the particle-based positive electrode provides valuable insight into the electro-chemo-mechanical behaviour that can be expected in solid-state batteries employing similar particle based architectures. Additionally, this integrated experimental-theoretical approach not only captures the rich coupling phenomena in structural batteries but also establishes a design-oriented modelling tool for next-generation multifunctional materials with built in strain sensing or morphing capabilities. This work has only investigated the voltage-strain coupling effect for small strains (quasi-static loading) where there is no risk for damage at these low strains and number of low cycles. Hence, for future work it still remains to investigate how structural battery cells respond to fatigue loading, dynamic loading and complex loading, such as non-uniform deformation.

CRediT authorship contribution statement

Rauan Al-Emrani: Writing – original draft, Visualization, Methodology, Investigation, Formal analysis. **Carl Larsson:** Writing – original draft, Visualization, Software, Methodology, Investigation, Formal analysis. **Clara Dahlberg:** Validation, Investigation. **Fredrik Larsson:** Writing – review & editing, Supervision, Methodology, Funding acquisition, Conceptualization. **Leif E. Asp:** Writing – review & editing, Supervision, Methodology, Funding acquisition, Conceptualization. **Johanna Xu:** Writing – review & editing, Writing – original draft, Visualization, Supervision, Methodology, Investigation, Conceptualization.

Declaration of competing interest

The authors declare that they have no known competing financial interests or personal relationships that could have appeared to influence the work reported in this paper.

Acknowledgment

The authors gratefully acknowledge financial support from the 2D-TECH VINNOVA Competence Center (Ref. 2019-00068); the U.S. Air Force Office of Scientific Research, European Office of Aerospace Research and Development (EOARD), under Awards No. FA8655-21-1-7038 and FA8655-25-1-7049; the Office of Naval Research, USA, under Awards No. N62909-22-1-2035 and N62909-22-1-2037; and the Swedish Research Council under Award No. 2023-04498.

Appendix A. Supplementary data

Supplementary material related to this article can be found online at <https://doi.org/10.1016/j.compositesb.2025.113286>.

Data availability

Data will be made available on request.

References

- [1] Asp LE, Greenhalgh ES. Structural power composites. *Compos Sci Technol* 2014;101:41–61.
- [2] Asp LE, Johansson M, Lindbergh G, Xu J, Zenkert D. Structural battery composites: A review. *Funct Compos Struct* 2019;1:042001.
- [3] Hermansson F, Edgren F, Xu J, Asp LE, Janssen M, Svanström M. Climate impact and energy use of structural battery composites in electrical vehicles—a comparative prospective life cycle assessment. *Int J Life Cycle Assess* 2023;28:1366–81.
- [4] Top 10 emerging technologies of 2025. 2025. https://reports.weforum.org/docs/WEF_Top_10_Emerging_Technologies_of_2025.pdf. Accessed online at.
- [5] Yang Z, Mu Y, Acauan LH, Fang J-H, Rogers M, Majeed MK, Luo J, Zhou Y. Understanding and recent advances on lithium structural batteries. *Chem Eng J* 2024;502:157772.
- [6] Chan KK, Lim GJH, Sutrisnoh NAA, Raju K, Srinivasan M. Toward a safe and high performance quasi-solid-state structural battery. *ACS Appl Energy Mater* 2024;7(20):9098–109.
- [7] Carlstedt D, Asp LE. Performance analysis framework for structural battery composites in electric vehicles. *Compos Part B: Eng* 2020;186:107822.
- [8] Chaudhary R, Xu J, Xia Z, Asp LE. Unveiling the multifunctional carbon fiber structural battery. *Adv Mater* 2024;2409725.
- [9] Siraj MS, Tasneem S, Carlstedt D, Duan S, Johansen M, Larsson C, Xu J, Liu F, Edgren F, Asp LE. Advancing structural battery composites: Robust manufacturing for enhanced and consistent multifunctional performance. *Adv Energy Sustain Res* 2023;2300109.
- [10] Asp LE, et al. A structural battery and its multifunctional performance. *Adv Energy Sustain Res* 2021;2:2000093.
- [11] Moyer K, et al. Carbon fiber reinforced structural lithium-ion battery composite: Multifunctional power integration for CubeSats. *Energy Storage Mater* 2020;24:676–81.
- [12] Xu J, Geng Z, Johansen M, Carlstedt D, Duan S, Thiringer T, Liu F, Asp LE. A multicell structural battery composite laminate. *EcoMat* 2022;4(3):e12180.

- [13] Harnden R, Peuvot K, Zenkert D, Lindbergh G. Multifunctional performance of sodiated carbon fibers. *J Electrochem Soc* 2018;165(13):B616.
- [14] Jacques E, Kjell MH, Zenkert D, Lindbergh G. Piezo-electrochemical effect in lithium-intercalated carbon fibres. *Electrochem Commun* 2013;35:65–7.
- [15] Jacques E, Lindbergh G, Zenkert D, Leijonmarck S, Kjell MH. Piezo-electrochemical energy harvesting with lithium-intercalating carbon fibers. *ACS Appl Mater Interfaces* 2015;7:13898–904.
- [16] Zenkert D, Harnden R, Asp LE, Lindbergh G, Johansson M. Multifunctional carbon fibre composites using electrochemistry. *Compos Part B: Eng* 2024;273:111240.
- [17] Wang C, Wang C, Huang Z, Xu S. Materials and structures toward soft electronics. *Adv Mater* 2018;30(50):1801368.
- [18] Rogers JA, Someya T, Huang Y. Materials and mechanics for stretchable electronics. *Science* 2010;327(5973):1603–7.
- [19] Song Y, Jung T, Rubloff GW, Stewart DM, Albertus P. Electrochemical-mechanical coupling strongly affects the performance of nanopore, thin-film, and solid-state batteries. *J Electrochem Soc* 2025;172(2):020529.
- [20] Monroe C, Newman J. The impact of elastic deformation on deposition kinetics at lithium/polymer interfaces. *J Electrochem Soc* 2005;152(2):A396.
- [21] Wu H, Huang Y, Xu F, Duan Y, Yin Z. Energy harvesters for wearable and stretchable electronics: From flexibility to stretchability. *Adv Mater* 2016;28(45):9881–919.
- [22] Baughman RH, Cui C, Zakhidov AA, Iqbal Z, Barisci JN, Spinks GM, Wallace GG, Mazzoldi A, Rossi DD, Rinzler AG, Jaschinski O, Roth S, Kertesz M. Carbon nanotube actuators. *Science* 1999;284(5418):1340–4.
- [23] Carlstedt D, Runesson K, Larsson F, Xu J, Asp LE. Electro-chemo-mechanically coupled computational modelling of structural batteries. *Multifunct Mater* 2020;3:045002.
- [24] Harnden R, Carlstedt D, Zenkert D, Lindbergh G. Multifunctional carbon fiber composites: A structural, energy harvesting, strain-sensing material. *ACS Appl Mater Interfaces* 2022;14(29):33871–80.
- [25] Carlstedt D, Runesson K, Larsson F, Jänicke R, Asp LE. Variationally consistent modeling of a sensor-actuator based on shape-morphing from electro-chemical–mechanical interactions. *J Mech Phys Solids* 2023;179:105371.
- [26] Newman J, Tiedemann W. Porous-electrode theory with battery applications. *AIChE J* 1975;21:25–41.
- [27] Doyle M, Fuller TF, Newman J. Modeling of galvanostatic charge and discharge of the lithium/polymer/insertion cell. *J Electrochem Soc* 1993;140(6):1526.
- [28] Doyle M, Newman J. The use of mathematical modeling in the design of lithium/polymer battery systems. *Electrochim Acta* 1995;40(13):2191–6, International symposium on polymer electrolytes.
- [29] Newman J, Thomas-Alyea KE. *Electrochemical systems*. Wiley: The ECS Series of Texts and Monographs; 2004.
- [30] Duan S, et al. Effect of lithiation on the elastic moduli of carbon fibres. *Carbon* 2021;185:234–41.
- [31] Larsson C, Larsson F, Xu J, Runesson K, Asp LE. Electro-chemo-mechanical modelling of structural battery composite full cells. *Npj Comput Mater* 2025;11(141).
- [32] Qi Y, Hector LG, James C, Kim KJ. Lithium concentration dependent elastic properties of battery electrode materials from first principles calculations. *J Electrochem Soc* 2014;161(11):F3010.
- [33] Tavano R, Spagnol M, Al-Ramahi N, Joffe R, Xu J, Asp LE. Mechanical characterisation of a structural battery electrolyte. *Polymer* 2024;312.
- [34] Gupta P, Üçel I, Gudmundson P, Olsson E. Characterization of the constitutive behavior of a cathode active layer in lithium-ion batteries using a bending test method. *Exp Mech* 2020;60(6):847–60.
- [35] Zhang W-J. Structure and performance of LiFePO₄ cathode materials: A review. *J Power Sources* 2011;196(6):2962–70.
- [36] Toray Composite Materials America, Inc. Accessed online at <https://www.toraycma.com/wp-content/uploads/T800H-Technical-Data-Sheet-1.pdf>.
- [37] Harnden R, Zenkert D, Lindbergh G. Potassium-insertion in polyacrylonitrile-based carbon fibres for multifunctional energy storage, morphing, and strain-sensing. *Carbon* 2021;171:671–80.
- [38] Carlstedt D, Rittweger F, Runesson K, Navarro-Suárez AM, Xu J, Duan S, Larsson F, Riemschneider K-R, Asp LE. Experimental and computational characterization of carbon fibre based structural battery electrode laminae. *Compos Sci Technol* 2022;220:109283.